




Influence of γ -ray exposure and dose dependent characteristics of (n)PbS–(p)Si hetero-structure

S. Aldawood^{1,*}, S. S. AlGamdi¹, S. A. Al Salman¹, M. S. AlGarawi¹, Turki S. ALKHURAIJI², and Syed Mansoor Ali^{1,*} 

¹Department of Physics and Astronomy, College of Science, King Saud University, P.O. BOX 2455, Riyadh 11451, Saudi Arabia

²King Abdulaziz City for Science and Technology (KACST), Nuclear Science Research Institute (NSRI), Directorate of International Cooperation (DIC), P.O. Box 6086, Riyadh 11442, Saudi Arabia

Received: 3 February 2021

Accepted: 15 March 2021

Published online:

8 April 2021

© The Author(s), under exclusive licence to Springer Science+Business Media, LLC, part of Springer Nature 2021

ABSTRACT

An (n)PbS–(p)Si hetero-structure was developed by preparing the lead sulfide (PbS) nanostructure thin films deposited on p-type Si wafer using the successive ionic layer adoption and reaction (SILAR) method. To investigate the radiation detection capability of (n)PbS–(p)Si hetero-structure. For this purpose, nanostructure, photoluminescence, optical bandgap and I–V characteristic have been examined with various γ -ray dose 0, 25, 50 and 75 kGy. X-ray diffraction of as deposited PbS comparing to the irradiated samples suggested that the crystalline is improved with the γ -ray up to 50 kGy dose. The morphology studies showed that the average sizes increased from 55 to 105 nm with increasing the incident γ -ray dose level and decreased with further increase of dose. Energy dispersive X-ray (EDX) analysis confirmed the elemental composition of the as deposited PbS thin films. The reflectance of the (n)PbS–(p)Si hetero-structure in the ultraviolet–visible–near infrared reflectance (UV–Vis–NIR) region reduced about 40% compared to as deposited sample. The band edge shifted to longer wavelengths with increasing dose level to 50 kGy, and the reverse trend is observed at 75 kGy dose. Photoluminescence (PL) spectra revealed that the (n)PbS–(p)Si hetero-structure received the lowest recombination rate at 50 kGy. The rectifying current–voltage (I–V) characteristics revealed impact of the γ -ray irradiation dose on the hetero-structure electrical parameters. The rectifying ratio and turn-on voltage reduced from 22.3 to 7.4 at 5 V, and 1.25–0.5 V with γ -ray irradiation, respectively. All ideality factors of as deposited and irradiated (n)PbS–(p)Si hetero-structure are greater than 4. The barrier height, series resistance exhibited minimum values (0.49 eV, 1.47 k Ω) and the largest saturation current 1.69×10^{-4} A, at 50 kGy.

Address correspondence to E-mail: sdawood@ksu.edu.sa; mansoor_phys@yahoo.com

1 Introduction

γ -ray is highly energetic electromagnetic radiation with large penetration power. It has the ability of repositioning the atoms of the irradiated materials from their lattice that may induced modifications in the properties of nanostructure materials [1]. The impact created by the γ -ray depends on the radiation dose, nature of irradiated host material and the incident angle of interaction [2, 3]. The perceived variations in nanostructure, electrical and optical properties of materials thin films due to the exposure to radiations may open a new window for the irradiated material for radiation detection and dosimetry applications. Understanding the induced modifications in the thin film properties, when they are irradiated by γ -ray, is required to design and improve the thin film and nanostructure based dosimeters [4, 5]. Several investigations have been reported on the properties of nanomaterials; however, insufficient studies on the nanostructure outcomes with large Z value nanomaterials have been examined with irradiation [6–10].

Semiconductor materials with comparatively high attenuation coefficients, large bandgap, good mobility, short carrier lifetime, as well as high resistivity exhibit a good radiation response [11]. Among them, lead-sulfide (PbS) may be a good candidate to observe the γ -ray impact due to its attractive properties, such as good electronic structure, large Z with an effective atomic number of 77 and tunable energy bandgap. Moreover, it can be grown in different dimensions [12, 13]. Recently, the radiation response of different semiconductor-based structures, such as Au/TiO₂ Schottky diode [14], Au/p-TiO₂/n-TiO₂ homojunction [15], Pt/TiO₂ metal–semiconductor–metal structure [16], and TiO₂/p-Si hetero-structure [17] have been investigated at different radiation doses. Compared to the above mention semiconductor based nanostructures, (n)PbS–(p)Si hetero-structures are incredibly simple to fabricate and are more effective for radiation detection as reported by [18].

The present investigations have described that hetero-structures properties may be meaningfully improved by γ -ray exposure due to the radiation induced influences, such as formation of defects states, charge trapping, deviations in the crystalline nanostructure on core deposited material, [19, 20]. Hence, the promising variations on the hetero-structures characteristics with and without γ -ray

irradiation should be systematically examined for improvement of considerable hetero-structures based detecting application. Recently, we have reported the variations influenced in the nanostructural, optical, and electrical investigation of lead sulfide thin films on glass substrate [21]. In this study, γ -ray irradiation impact on the nanostructure, current–voltage, optical, surface and morphological characteristics of (n)PbS–(p)Si hetero-structures as a diode and their correlations with γ -ray irradiation dose have been thoroughly investigated. Moreover, the novelty of present work is to analyzed the impact of γ -ray irradiation (n)PbS–(p)Si hetero-structures at different dose levels. The PbS thin film is a nanostructure material with narrow-gap, high attenuation coefficient, large mobility and used as a material for temperature sensors, photodetectors, photoresistors, and selective sensors. Such type of material is good candidate to understanding of the irradiation effects for γ -ray sensor application. To understand the impact of irradiation in any structural, optical and electrical modification in the PbS thin films owing to γ -ray irradiation dose, sample characteristics such as crystallinity, morphology, optical bandgap energy, photoluminescence and electrical changes were studied. To the best of our current knowledge, such type of study in which the irradiation with high-energy γ -ray to hetero-structures, with impact on dislocation of lattice with ionization damages that create defects in the PbS and produce the carrier trapping interface of hetero-structures is not investigated previously.

2 Materials and methods

2.1 Fabrication of the hetero-structures

To assemble the (n)PbS–(p)Si hetero-structure, PbS thin films were developed on the p-type Si with a (100) orientation wafer. To eliminate the contaminants and the SiO₂ layer on the wafer surface, it was washed away with solution of dilute Hydrofluoric acid (HF) and deionized water (DIW) and then dehydrated by purging with nitrogen. Lead nitrate (Pb(NO₃)₂ with purity of 99.9% and sodium sulfide (Na₂S with purity > 99%), purchased from Sigma Aldrich, were used for the deposition of PbS thin films. Two precursor solutions as the cationic (Pb²⁺) source (0.5 M solution of Pb(NO₃)₂ in DIW) and as the anionic (S^{2−}) source (0.5 M solution of Na₂S in

ethanol) were prepared. The cleaned wafer was immersed in the cationic solution for 1 min, thereby starting an adsorption of Pb ions on clean Si wafer and then soaked with DIW and heated at 100 °C. Afterward, it was dipped in an anionic solution for 1 min to react S^{2-} with Pb^{2+} ions, rinsed with ethanol and heated at 100 °C to dry. Consequently, a SILAR deposition cycle of PbS preparation was finished. To achieve the appropriate thickness, 20 cycles were completed, followed by annealing at 300 °C under a vacuum condition.

2.2 Thickness measurement

The thickness of the deposited PbS thin films on Si was calculated using the relation:

$$t = M/\rho A, \quad (1)$$

where ' M ' is the mass of deposited PbS, A is area of the film, and $\rho = 7.6 \text{ g/cm}^3$ of PbS. The deposited thickness of PbS was measured to be approximately 237 nm.

2.3 γ -ray irradiation

Three sample (total of four) of the (n)PbS–(p)Si hetero-structure was exposed to γ -ray irradiation with various radiation doses in the range of 0–75 kGy using source ^{60}Co with an energy of 1.31 MeV and activity of 7.328 kGy/h, (Model SC220E, MDS Nordion). The samples were positioned at 6.5 cm from the source in a closed chamber.

2.4 Characterization

The phase structural investigations of the pristine and γ -ray irradiated hetero-structure were studied by X-ray diffraction using Panalytical X'Pert3 with an X-ray source of $\text{CuK}\alpha$. The morphologies of hetero-structures samples were explored by field emission scanning electron microscopy (FESEM) using JEOL. The diffuse reflectance spectra were recorded using an integrating sphere in spectrophotometer (JASCO-V 670) and spectrofluorometric (JESCO FP-8200) is used to performed photo emission spectra. For electrical properties, the Platinum (Pt) contact electrodes were prepared on the (n)PbS and (p)Si sides of hetero-structure via sputtering with active area of 0.25 cm^2 and thickness of about 50 nm. The dark environment I–V characteristics of hetero-structure before

and after irradiation were measured in a by semiconductor characterization system (KEITHLEY 4200).

3 Results and discussion

Figure 1 illustrates the XRD results of the (n)PbS–(p)Si hetero-structure with different γ -ray doses from 0 to 75 kGy. In Fig. 1, five diffraction peaks are detected for PbS with (111), (200), (220), (311), and (422) indexes, at positions 26.43°, 30.13°, 44.14°, 49.73°, and 78.74°, respectively. The peaks represented by (111) and (200) appeared to the prominent peak as compare to the other, that indicates the structural orientation. The indexed XRD peaks approve the cubic structure of PbS, which corresponds to JCPDS reference no. 03-066-0020. The investigated results are well consistent with the data on PbS thin films [22]. In addition, the peak at positions 31.34° corresponds to the (110) reflection with the low-intensity PbO (JCPDS card # 03-610). The high intensity of Si diffraction peak (400) arising from wafer at positioned 69.42° is detected. It can be observed that the intensity of the preferred diffraction increases with the γ -ray dose, which may be due to the increased heat as the incident radiation energy increases. The increasing temperature induces the enhancement of the crystallization of PbS thin films.

The Scherrer formula [41] is employed to compute the crystallite size (D) of the pristine and γ -ray irradiated samples using the (111) plane:

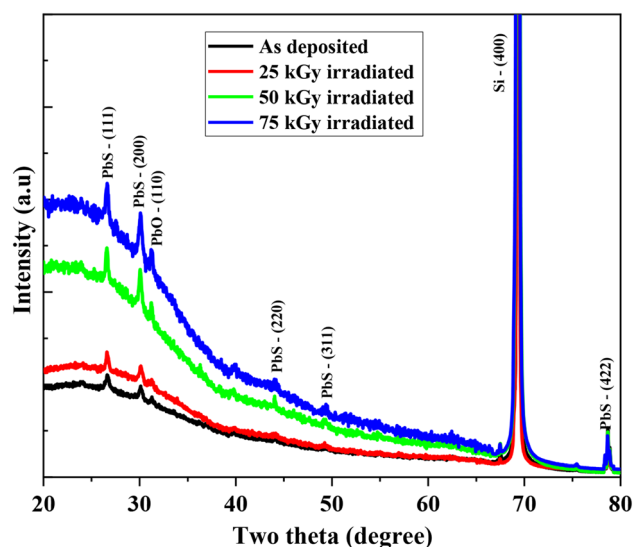


Fig. 1 X-ray diffraction spectra with and without γ -ray irradiated (n)PbS–(p)Si hetero-structure

$$D = \frac{0.9\lambda}{\beta \cos \theta}, \quad (2)$$

where ($\lambda = 1.54 \text{ \AA}$) is the incident X-ray wavelength, ' β ' is the full width at half maxima (FWHM), and ' θ ' is the angle for the considered peak. The estimated crystallite sizes for all the samples are tabulated in Table 1. It is clear from the calculated sizes that the crystallite size increases with the γ -ray dose up to 50 kGy, after which it starts to decrease as the incident γ -ray dose increases further (75 kGy). This upsurge in the crystallite size with the γ -ray irradiation is associated with the agglomeration of small crystallites, which leads to the establishment of big crystallites [20]. The decrease in the crystallite size with a high γ -ray dose may be due to the high-energy transfer in the host material, which explains the breaking of the large crystallites into small fragments. The lattice parameter of the cubic structure is determined using Millar indices of the (111) plane [23]:

$$a = d(h^2 + k^2 + l^2)^{1/2}, \quad (3)$$

where ' a ' is the lattice parameter, ' (h, k, l) ' are the indices of plane, and ' d ' is the inter planer spacing. The variation of the measured lattice constant from the bulk material ($a_0 = 5.936 \text{ \AA}$) reveals that the pristine PbS thin films were under strain. The normal stress and micro strain in the pristine and γ -ray irradiated thin films were determined using the following relations [24]:

$$S = \frac{\left\{ \frac{a_0 - a}{a_0} \right\} Y}{2\sigma}, \quad (4)$$

$$\varepsilon = \frac{\beta}{4 \tan \theta}, \quad (5)$$

where $Y = 70.2 \text{ GPa}$ is Young modulus and $\sigma = 0.28$ is Poisson ratio of PbS bulk material. The decrease in the stress and structural strain is due to the increase in the crystallite size, increase in the lattice dislocation, and narrowing of the XRD diffraction. Table 1 demonstrates the deviation of stress with different values of incident γ -ray doses. Noteworthy, the calculated stress and micro strain values decrease as the γ -ray dose increases up to 50 kGy. The reduction of the micro strain is responsible for the increase in the XRD peak intensities [25]. The lattice imperfection (dislocation density) was determined using the equation [26]:

Table 1 Nanostructural results with and without γ -ray irradiated (n)PbS–(p)Si hetero-structure

γ -ray (kGy)	Two theta (degree)	FWHM (rad.)	Planner spacing (\AA)	Lattice parameter (\AA)	Volume (\AA^3)	Crystallite size (nm)	Stress (N/m^2) $\times 10^9$	Strain $\times 10^{-3}$	Dislocation density ($1/\text{nm}^2$) $\times 10^{-3}$	No. of crystallite $\times 10^{16}$	Crystallite density ρ (g/cm^3)	Surface area (cm^2/g)
0	26.71	0.0075	3.333	5.767	191.80	18.983	3.567	7.9	2.78	3.216	4.15	76.26
25	26.63	0.0056	3.343	5.784	193.51	25.504	3.208	5.9	1.54	1.326	4.11	57.26
50	26.54	0.0045	3.354	5.803	195.45	31.383	2.801	4.81	1.02	0.712	4.07	47.00
75	26.62	0.0057	3.344	5.786	193.72	24.730	3.163	6.09	1.64	1.454	4.10	59.11

$$\delta = \frac{1}{D^2} \quad (6)$$

According to this Eq. (9) that the lattice imperfection or dislocation density of samples is indirectly associated to the square of the crystalline size. It is indicated in Table 1, the calculated dislocation densities of the unirradiated sample are smaller than those of the γ -ray irradiated samples. The minimum value of the lattice imperfection was found for the 50 kGy γ -ray dose with the smallest crystallite size. These dislocations in the PbS gradually transfer to close the grain boundaries and become neutralized [27]. The number of crystallites per unit area (N) of the pristine and γ -ray irradiated PbS was estimated as follows [28]:

$$N = \frac{t}{D^3} \quad (7)$$

As reported in Table 1, N decreases as the incident γ -ray radiation dose increases up to 50 kGy, after which it increases with a further increase in the γ -ray dose. The crystalline density (ρ) of the pristine and γ -ray irradiated samples were determined by means of Eq. (8) and are given in Table 1:

$$\rho = \frac{2M}{N_A V} \quad (8)$$

where ($N_A = 6.02 \times 10^{23}$) is stand for Avogadro's number, 'M' is the molecular mass of PbS (239.39 g/mole) and 'V' is the volume unit cell of cubic structure. Comparing all the γ -ray irradiated doses, the crystallite densities along the (111) plane are the lowest at 50 kGy. This might be due to the enhancement in the nucleation, that may account for the growth in the crystallite and reduction in surface area. Surface area (S) of crystallite PbS with the effect of γ -ray irradiation was calculated and is given in Table 1:

$$S = \frac{6000}{\rho \times D} \quad (9)$$

The Eq. (9) is used to measure for spherical particles, as detected in the prepared thin film. Lowest specific area observed with a large crystallite size at the 50 kGy γ -ray dose, which may be due strain generated during the γ -ray irradiation.

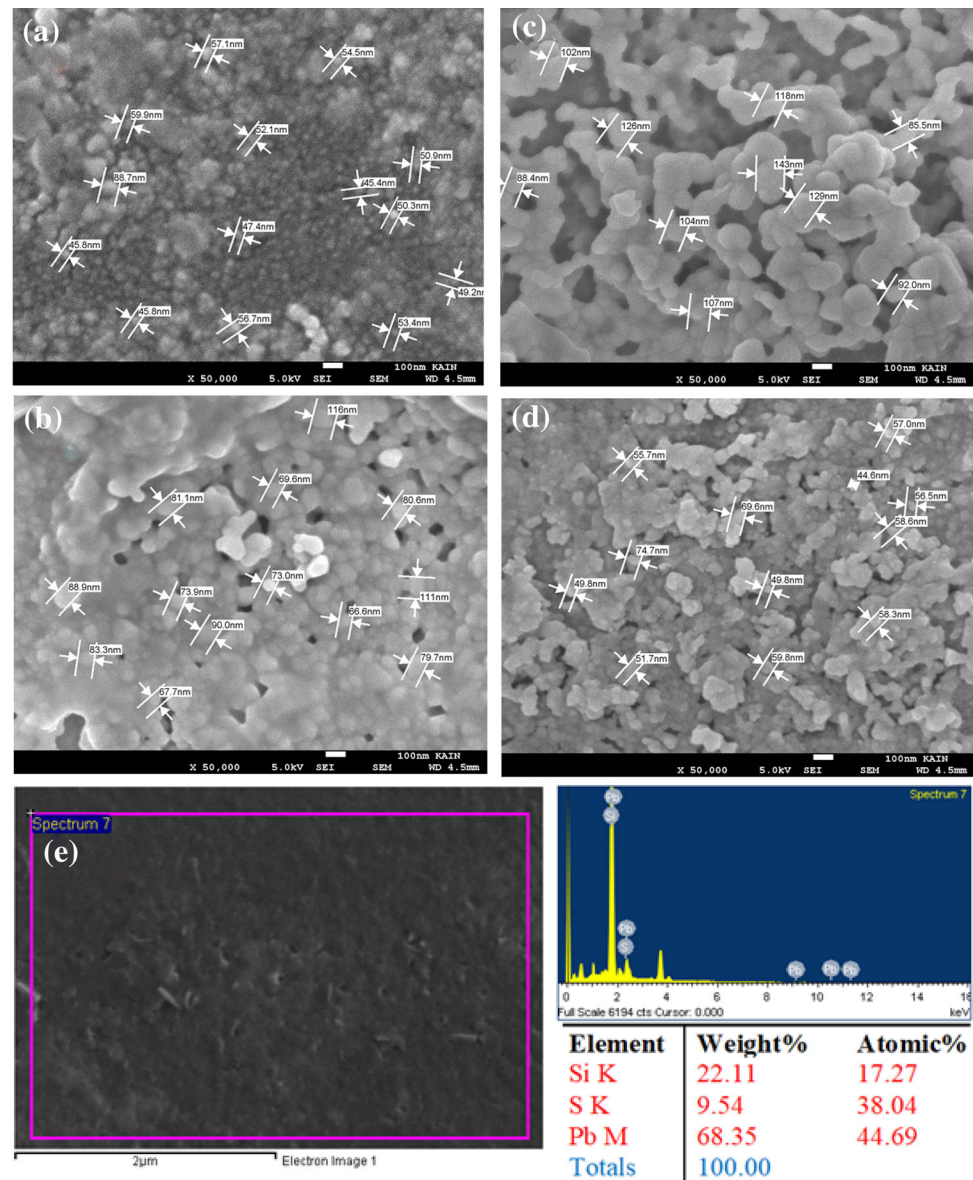
Figure 2a–d shows the FESEM morphologies of the pristine and γ -ray irradiated (n)PbS–(p)Si hetero-structure. It can be observed in Fig. 2a, that the PbS thin film is densified grain in spherical granular shape with

an estimated average diameter of ~ 55 nm and that they consistently cover all area of Si wafer. After γ -ray irradiation with the dose increased up to 50 kGy, the grain size also increased to 105 nm, which may be due to the agglomeration of small grains and formed cluster of particles in different shapes, as shown in Fig. 2b, c. At a high γ -ray dose (75 kGy), significantly high energy is transferred to the PbS lattice, that is changed to the kinetic energy of the particles; this may be the reason of thermal spurts. By this principle, the grain size decreases to 42 nm as compared to the case of the 50 kGy-irradiated sample, as displayed in Fig. 2d. The FESEM consequences are in well agreement with the XRD outcomes. At 50 kGy γ -ray irradiation dose, the agglomeration of grains increases the atomic diffusion on the surface, which consequently leads to the formation of extra atoms sideways to the surface grown larger compact grains and enhancement of the mobility and crystallinity of the PbS thin films [29]. The EDX analysis results of the as-deposited (n)PbS–(p)Si hetero-structure are illustrated in Fig. 2e. Which indicates the energy peaks corresponding to Pb, S, and Si that confirms the elemental composition of the prepared hetero-structure (see inset of Fig. 2e).

When (n)PbS–(p)Si is irradiated by γ -ray, γ -ray photons may affect the optical properties of the junction by creating defects inside the bandgap. These induced defects may alter the results of the γ -ray sensing experiment. Therefore, the influence of the γ -ray irradiation on the hetero-structure was studied with different γ -ray doses to elucidate the impact of the radiation on the optical properties. By varying the γ -ray radiation dose, it was demonstrated that the radiation changes the diffuse reflectance of the (n)PbS–(p)Si hetero-structure significantly, as shown in Fig. 3a in the wavelength range of 200–1100 nm. It is detected that PbS has less reflectance from 200–700 nm with band edge at 848 nm. For the pristine sample, the band edge is shifted toward longer wavelengths with increasing the γ -ray dose from 0 to 50 kGy; thereafter, it exhibited the reverse behavior for high doses. The normalized reflectance of PbS thin films is efficiently reduced after γ -ray irradiation, and the minimum reflectance is achieved at the dose of 50 kGy, may be due to the increase in the defects generated by the irradiation in the host material and decrease in the non-homogeneity of the prepared thin films.

The bandgap can be accurately estimated using the reflectance spectra. According to the theory of

Fig. 2 FESEM images **a** without irradiation, **b** 25 kGy, **c** 50 kGy and **d** 75 kGy γ -ray irradiated (n)PbS-(p)Si hetero-structure. **e** Represents the EDX analysis of the as deposited (n)PbS-(p)Si hetero-structure



Kubelka and Munk, the absorption coefficient from the reflectance can be corresponded to the equation [30, 31]:

$$F(R) = \frac{(1 - R)^2}{2R} \quad (10)$$

where 'R' is reflectance, and $F(R)$ is Kubelka–Munk function, that can be converted into the absorption coefficient (α) by Eq. (14). The energy bandgap is obtained using Tauc's equation [32, 33]:

$$\alpha = \frac{FR}{t} \quad (11)$$

$$(\alpha h\nu) = \frac{F(R)h\nu}{t} = B(h\nu - E_g)^n \quad (12)$$

where 'B' is constant independent on energy of energy, ' E_g ' is the optical bandgap, ' h ' is Planck's constant, ν is the incident photon frequency and n is a constant that influenced by on the kind of electron transition; for direct transition, the value of $n = 1/2$. In Fig. 3b, the straight part of plots $(\alpha h\nu)^2$ vs $(h\nu)$ is extended to the x-axis and provides the values of the energy bandgap. The variation of the estimated optical bandgap values with γ -ray irradiated dose of the (n)PbS-(p)Si hetero-structure is depicted in the inset of Fig. 3b. It is observed that the bandgap significantly reductions as the γ -ray dose rises up to 50 kGy, after which it increases at 75 kGy. The growth in the optical bandgap indicates that the

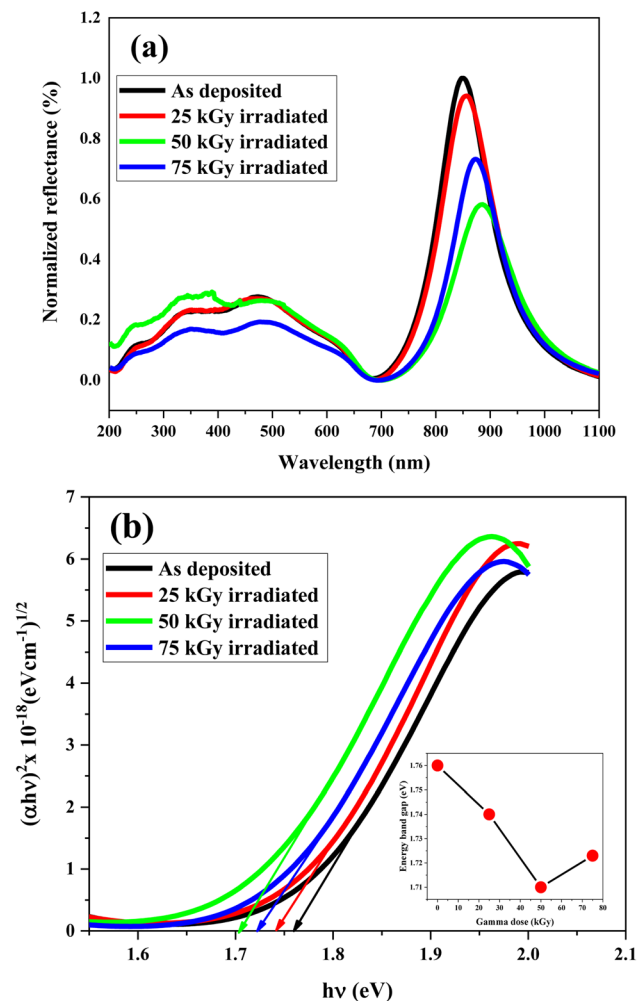


Fig. 3 **a** UV–Vis diffuse reflectance spectra and **b** Tauc's Plot for the bandgap of (n)PbS–(p)Si hetero-structure with and without γ -ray irradiation and (inset) shows the variation of bandgap with the γ -ray dose

energy gap among the conduction and valence bands are being enlarged by the γ -ray irradiations. Subsequently, the defects or trap level of the PbS near to the conduction or valence edge, which can have improved population of charge carriers. This phenomenon were studied for other reported γ -ray irradiated materials, e.g., AgInSe₂ [34] thin films and ZnO nano rods [35]. Maity et al. [36] reported the enhancement of optical bandgap due to the defects produced in the bandgap and the decrease in the approachability of charge carriers in the PbS.

The radiation induced crystal defects variation of the (n)PbS–(p)Si hetero-structure caused by exposure to different γ -ray irradiation doses can be studied by evaluating photoluminescence (PL) analysis. Figure 4a depicts the PL varieties for all samples, where

the structural deficiencies can be detected at the excitation of 675 nm. It is noticeable from the PL spectra that the pristine and γ -ray irradiated (n)PbS–(p)Si hetero-structure have one inherent PL peak at 761.67 nm in different intensities. The extensive PL peak is associated with the charge transition in PbS from the conduction to valence band. After γ -ray irradiation, a hump appears at 778 nm, which is attributable to the deficiency linked to the charge capturing inside defects. The clear reduction in the full width at half maxima value up to 50 kGy of the PL peak, as shown in Fig. 4b, can be attributed to the good improvement in the crystallinity of the structure with γ -ray irradiation [37], and the decrease in the PL intensity with growing γ -ray doses is attributable to the reduction of the charges recombination rate [21]. The γ -ray irradiation generates traps and induced the localized energy level inside energy bandgap, and acting as recombination centers. These traps influence the generated carrier lifetime and their mobility. By γ -ray irradiation charge carrier defects density is increased, which increased the significant reduction of the carrier recombination rate and caused to decreased of PL intensity [38]. The blue shift in the PL peak with increasing the γ -ray doses is associated with the band structure modifications in the deposited PbS. The irradiated (n)PbS–(p)Si hetero-structure with 50 kGy γ -ray dose has the lowest recombination rate, and it is more crystalline than all the samples.

For the reverse and forward biased (I–V) characteristics of (n)PbS–(p)Si hetero-structure, the voltage is applied between the p-Si wafer and the PbS contact in the range of – 10 V to 10 V. The applied voltage scheme is shown in Fig. 5a. The room-temperature I–V characteristics of the (n)PbS–(p)Si hetero-structure with and without γ -ray radiation (0–75 kGy) in a dark environment are illustrated in Fig. 5b. The I–V characteristics show the noticeable rectifying behavior in the positive bias presenting “on state” with high current, whereas in the negative, an “off state” is demonstrated with low current. The rectification ratio decreases from 22.3 to 7.4 at 5 V, and the turn-on voltage varies from 1.25 to 0.5 V with γ -ray irradiation. This decrease in the turn-on value results in low power consumption [39]. It can be observed that the I–V characteristics of the (n)PbS–(p)Si hetero-structure demonstrate the parallel shift in both forward and reverse biases after γ -ray exposure. The current values increase in both the polarities up to 50 kGy, after which they decrease with more increase in the γ -

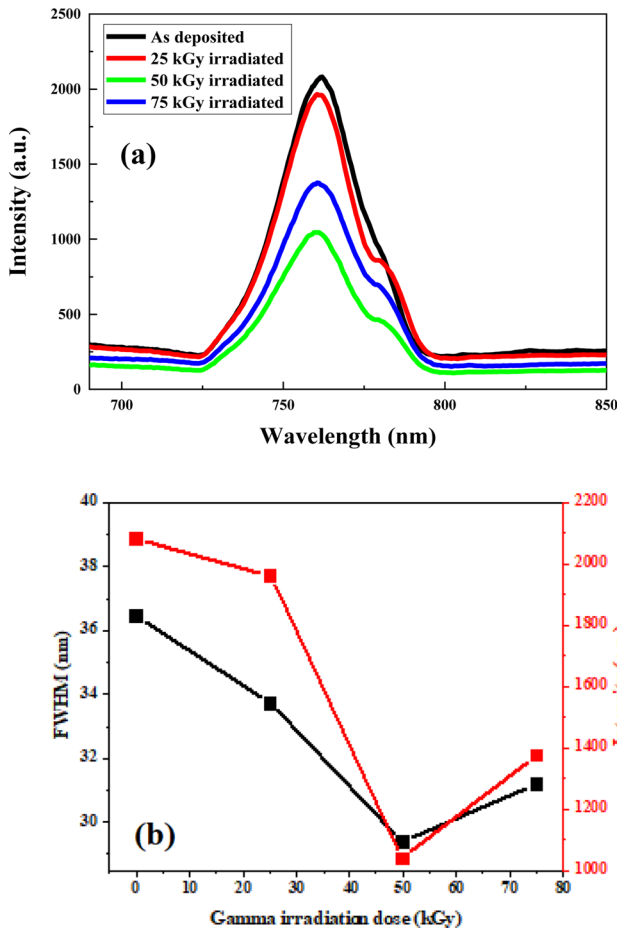


Fig. 4 **a** PL spectra of the (n)PbS–(p)Si hetero-structure with different gamma irradiation dose. **b** Represents variation of FWHM and intensity of PL peaks as a function of gamma dose

ray dose. The enhancement of current in forward and reverse direction can be linked with the reduction of the charge pair recombination rate, which was already observed in the PL analysis of the γ -ray radiation electron traps defects inside the forbidden gap [40].

To compute the ideality factor (n), barrier heights (Φ_b), and saturation current (I_s) of the (n)PbS–(p)Si hetero-structure with and without γ -ray irradiation, the I–V response of the hetero-structure under biasing can be modeled using the ideal diode equation [41]:

$$I = I_s \left(e^{\left(\frac{V}{nKT} \right)} - 1 \right) \quad (13)$$

where ' k ' is the Boltzmann's constant, ' V ' is the applied voltage across the junction and ' T ' is room temperature. The values of the saturation current are calculated from the Y-intercept of the linear portion

of the forward bias $\ln(I)$ – V graph (Fig. 5c), as given in the following relation [41]:

$$I_s = AA^* \exp \left(\frac{-q\phi_b}{kT} \right) \quad (14)$$

where ' A ' is area of thin films, ' A^* ' is for p-type Si the value is 31.6 A/cm^2 material called Richardson constant [40]. The ideality factor is calculated from the gradient of the straight line of the $\ln(I)$ – V graph using the following equation [42]:

$$n = \frac{q}{kT} \left(\frac{dV}{d(\ln I)} \right) \quad (15)$$

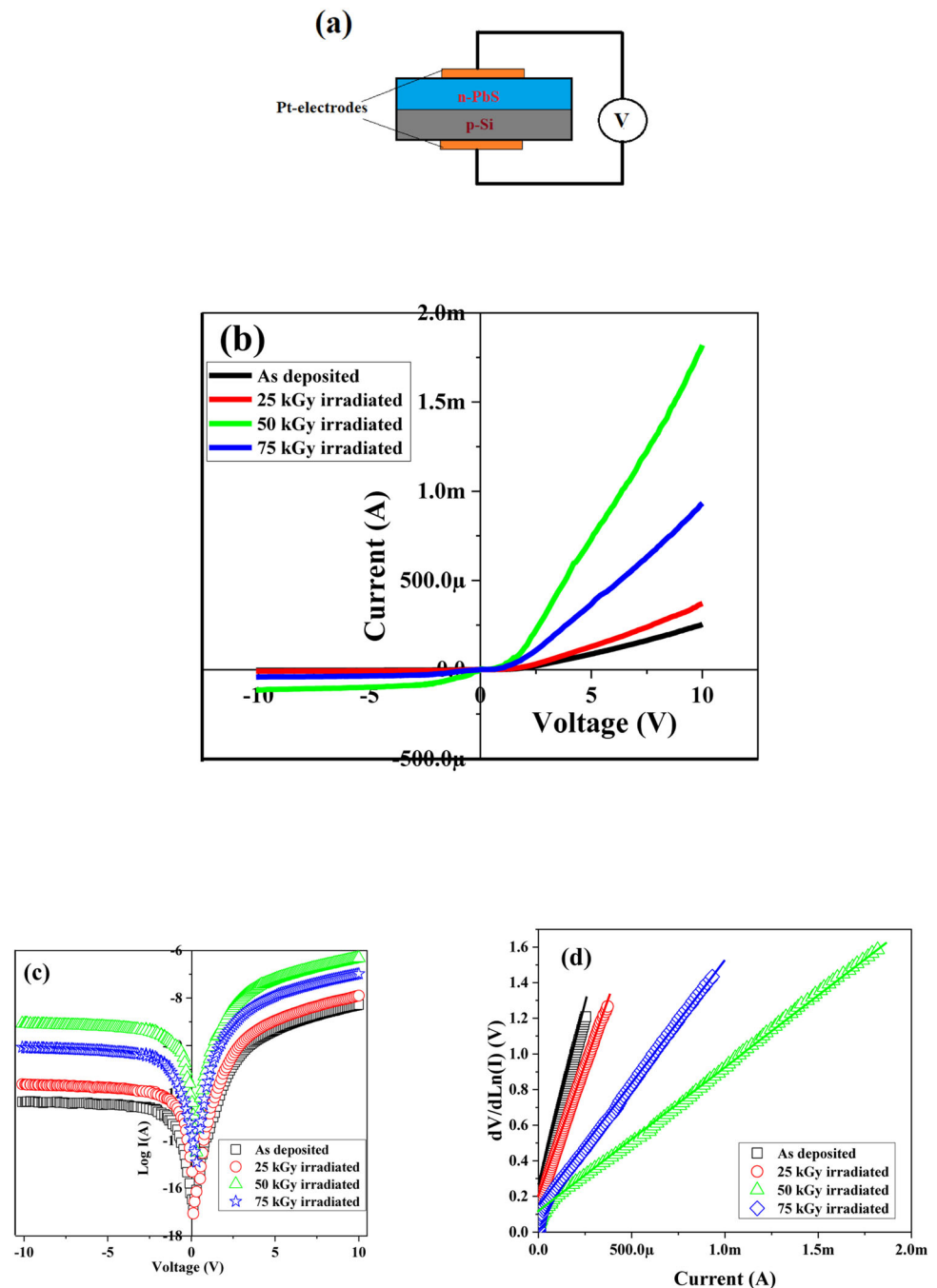
Using the calculated values of I_s , the barrier height can be determined by the relation [43]:

$$\phi_b = \frac{kT}{q} \ln \left(\frac{AA^*}{I_s} \right) \quad (16)$$

The ideality factor value of the pristine and γ -ray irradiated samples is greater than the perfect condition ($n = 1$). The larger values of the ' n ' indicate that the charge transport phenomena is not conquered to the thermionic emission, but by other processes for example tunneling through traps or by electron–hole recombination [44]. The measured electrical parameters of all the PbS samples are provided in Table 2. The increase in the values of ' n ' and ' I_s ' indicates that the presence of dynamic equilibrium due to the dissimilar attitudes of defect creation and the inhaling caused by the exposure to γ -ray. Ali et al. [20] reported comparable findings. The barrier potential is in fact the intrinsic blockade at the junction of the PbS thin film and the p-Si wafer. The barrier height decreases as the γ -ray doses increase to a certain level, after which it begins to increase at 75 kGy. The increase of in the current in both direction demonstrates the improvement of charge mobility across the (n)PbS–(p)Si hetero-structure [44]. The series resistance (R_s) is a significant parameter of the hetero-structure. The I–V characteristics deviate meaningfully with the change of the ideality factor, that may due to the effect of the series resistance (R_s). The ' R_s ' and ' n ' of the hetero-structure can be derived by Cheungs' method [45]:

$$\frac{dv}{d(\ln I)} = IR_s + n \left(\frac{kT}{q} \right) \quad (17)$$

Fig. 5 **a** Structure and applied voltage scheme of the (n)PbS–(p)Si hetero-structure, **b** I – V characterization, **c** $\ln(I)$ – V graph, and **d** Cheung's plot of (n)PbS–(p)Si hetero-structure with and without γ -ray irradiation with different dose



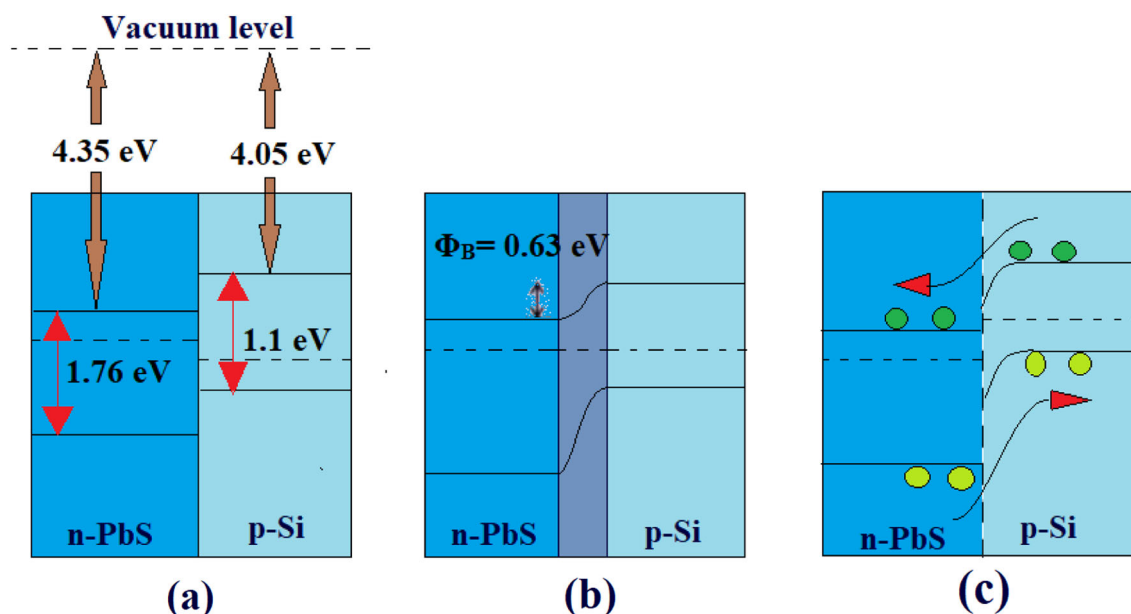
To determine the ' R_s ' and ' n ', the graph of $dV/d(\ln I)$ against I , established on equation 20, is plotted as shown in Fig. 5d. The gradients of the linear line give the series resistance, and the intercepts correspond to the ' n ' [45]. Table 2 also provides the values of the ' R_s ' and ' n ' calculated by Cheungs' method. The variation between the calculated values of the ' n ' from the both way presented above is due to the existence of the ' R_s ' and the barrier potential at the junction [46]. The ' R_s ' decrease as the incident γ -ray

doses increase, and the minimum values are exhibited at 50 kGy. This decrease is probably due to the decrease in the trap concentration at the junction between the PbS film and the Si wafer.

The carrier transport mechanisms of (n)PbS–(p)Si hetero-structure of pristine and γ -ray irradiation under applied voltage can be described using energy band banding, as depicted in Fig. 6. The valance band (VB) and conduction band (CB) p-Si and PbS are shown in Fig. 6a, where the values of the electron

Table 2 Computed electrical parameters by current–voltage characteristic of the (n)PbS–(p)Si hetero-structure

γ -ray irradiation (kGy)	Ideality factor		Saturation current ($A \times 10^{-4}$)	Barrier potential (eV)	Series resistance (k Ω)
	lnI–V	Cheung's method			
As-deposited	4.53	4.82	6.86	0.63	4.63
25	4.76	4.96	7.74	0.54	3.96
50	4.97	5.05	9.69	0.49	1.47
75	4.69	4.79	8.37	0.53	2.63

**Fig. 6** **a** Band-edge alignment of the energy band of PbS and Si, **b** band bending at 0 V bias, **c** carrier transportation upon applying a bias

affinity and the bandgap of PbS are 4.35 and 1.76, respectively [47]. When the thin films deposited on the Si substrate, electrons drift from Si to PbS and holes move in the opposite direction. With zero biased at equilibrium, the Fermi level energy reached at same level and an intrinsic electric field is generated at the interface and energy band bending is occurred as revealed in Fig. 6b. The banding energy barrier for n-type charge carrier is $\Delta E_c = \chi(\text{PbS}) - \chi(\text{Si}) = 4.35 - 4.05 = 0.3$ eV, and p-type charge carrier is $\Delta E_v = E_g(\text{PbS}) + \Delta E_c - E_g(\text{Si}) = 1.76 + 0.3 - 1.10 = 0.96$ eV. Evidently, the banding energy barrier for VB is larger as compare to the CB. Therefore, the n-type carrier transported more during the forward applied voltage across (n)PbS–(p)Si hetero-structure. Hence (n)PbS–(p)Si delivers a large forward current and a small reverse current. After γ -ray irradiation, the energy bandgap of PbS decreases. Therefore, the energy barrier for the hole is increased and more electrons are transformed

during the forward bias. By applying a reverse bias, the Fermi level increases toward greater values, that can improve the barrier potential at the interface region steadily and as a consequence in the growth of the barrier height. In the gamma irradiated samples, the carriers are generated in both Si and PbS and nonequilibrium is formed in the heterojunction, as demonstrated in Fig. 6c. More gamma dose generates more charge carriers and contributed in the forward and reverse up to 50 kGy. At high gamma dose the current is decreased, which may be due to the charge trapping in the defects state.

4 Conclusions

Nanostructured PbS thin films has been grown on boron doped Si (p-type) wafer by the SILAR technique, and the prepared PbS and Si wafer were act as n-type and p-type semiconductors to construct a

(n)PbS–(p)Si hetero-structure. The impact of the γ -ray radiation dose on the nanostructure, photoluminescence, optical and I–V characteristic of the (n)PbS–(p)Si hetero-structure was inspected. The γ -ray photon energy attenuated considerably in the range of 1–31 keV and subsequently decreased to the minimum level. The XRD results confirmed the cubic structure of PbS and revealed that its crystallinity in the preferred orientation improved with the γ -ray dose. FESEM results exposed the PbS thin films were homogeneous and that the grain size increased from 27 nm to 65 after γ -ray irradiation. At 50 kGy, the agglomeration of grains increased the atomic diffusion on the surface, resulting in the formation of extra atoms sideways to the surface that grew relatively large compact grains. EDX analysis confirmed the stoichiometry of the fabricated hetero-structure. The optical energy bandgap of the deposited thin film firstly decreased from 1.78 to 1.70 eV, and then increased to 1.72 eV after γ -ray irradiation. The PL spectra showed the decreased PL intensity and the blue shift in the PL peak was ascribed to the electronic structure modifications in the PbS with increasing the γ -ray dose. The I–V characteristics of as deposited and γ -ray irradiated hetero-structure showed a diode behavior. The increase in the ideality factor and the saturation current indicated the existence of dynamic equilibrium was due to the different attitudes of defect creation and inhalation due to γ -ray irradiation. The reduction in the series resistance with increasing γ -ray doses up to 50 kGy may be due to the decrease in the density of the trap states at the interface between the PbS film and the Si wafer. This may improve the (n)PbS–(p)Si hetero-structure for application in γ -ray dosimetry.

Acknowledgements

The authors extent their appreciation to the Deputyship for Research and Innovation, “Ministry of Education” in Saudi Arabia for funding this research work through the project number IFKSURG-1441-315.

References

1. M. Mohil, G.A. Kumar, *J. Nano Electron.* **2**, 2018 (2013)
2. L.I. Ivanov, Y.M. Platov, Cambridge International Science Publishing, UK (2004)
3. E. Colby, G. Lum, T. Plettner, J. Spencer, *I.E.E.E.T. Nucl. Science* **49**, 2857 (2002)
4. K. Arshak, O. Korostynska, *Sens. Rev.* **26**, 70 (2006)
5. S. Kaya, E. Yilmaz, Influences of Co-60 gamma-ray irradiation on electrical characteristics of Al₂O₃ MOS capacitors. *J. Radioanal. Nucl. Chem.* **302**, 425–431 (2014)
6. S. Kaya, E. Yilmaz, A. Aktag, J. Seidel, Characterization of interface defects in BiFeO₃ metal-oxide-semiconductor capacitors deposited by radio frequency magnetron sputtering. *J. Mater. Sci.-Mater. Electron.* **26**, 5987–5993 (2015)
7. S. Kaya, E. Yilmaz, A. Kahraman, H. Karacali, Frequency dependent gamma-ray irradiation response of Sm₂O₃ MOS capacitors. *Nucl. Instrum. Method B* **358**, 188–193 (2015)
8. R. Lok, S. Kaya, H. Karacali, E. Yilmaz, A detailed study on the frequency-dependent electrical characteristics of Al/HfSiO₄/p-Si MOS capacitors. *J. Mater. Sci. Mater. Electron.* **27**, 13154–13160 (2016)
9. R. Lok, S. Kaya, E. Yilmaz, Thermal phase separation of ZrSiO₄ thin films and frequency-dependent electrical characteristics of the Al/ZrSiO₄/p-Si/Al MOS capacitors. *Semicond Sci. Tech.* **33**, 055007 (2018)
10. S.D. Del Sordo, L. Abbene, E. Caroli, A.M. Mancini, A. Zappettini, P. Ubertini, Progress in the development of CdTe and CdZnTe semiconductor radiation detectors for astrophysical and medical applications. *Sensors* **9**, 3491–3526 (2009)
11. J. Perkins, H. Krawczynski, P. Dowkontt, Characterizing Imarad CZT detectors With time resolved anode and cathode, Proceedings of the 13th International I.E.E.E. Workshop on Room-Temperature Semiconductor X- and Gamma-Ray Detectors (2003)
12. M. Urdaneta, P. Stepanov, I. Weinberg, Irina Pala2 and Stephanie Brock2Quantum Dot Composite Radiation Detectors 1Weinberg Medical Physics LLC 2Wayne State University USA (2021)
13. S. Chakrabartty, A. Mondal, M.B. Sarkar, B. Choudhuri, A.K. Saha, A. Bhattacharyya, TiO₂ nanoparticles arrays ultraviolet-A detector with AU schottky contact. *IEEE Photon Technol. Lett.* **26**, 1065–1068 (2014)
14. A. Hazra, P.P. Chattopadhyay, P. Bhattacharyya, Hybrid fabrication of highly rectifying p-n homojunction based on nanostructured TiO₂. *IEEE Electron. Device Lett.* **36**, 505–507 (2015)
15. M. Zhang, D. Zhang, F. Jing, G. Liu, K. Lv, J. Zhou, S. Ruan, Fast decay time and low dark current mechanism in TiO₂ ultraviolet detector. *IEEE Photon Technol. Lett.* **27**, 54–57 (2015)

16. S.M. Ali, Gamma induced effects on structural, optical and electrical properties of n-TiO₂/p-Si heterojunction. *J. Mater. Sci. Mater. Electron.* **28**, 16314–16320 (2017)
17. H. Khlyap, *Physics and Technology of Semiconductor Thin Film-Based Active Elements and Devices* (Bentham Science Publishers, Sharjah, 2009).
18. S. Lotfy, A. Atta, E. Abdeltwab, Comparative study of gamma and ion beam irradiation of polymeric nanocomposite on electrical conductivity. *J. Appl. Polym. Sci.* **135**, 46146 (2018)
19. A.G. El-Shamy, W.M. Attia, K.M. Abd El Kader, Enhancement of the conductivity and dielectric properties of PVA/Ag nanocomposite films using gamma irradiation. *Mater. Chem. Phys.* **191**, 225–229 (2017)
20. S.M. Ali, *J. Mater. Sci. Mater. Electron.* **28**, 16314 (2017)
21. S.M. Ali, M.S. AlGarawi, S. Aldawood, S.A. Al Salman, S.S. AlGamdi, Influence of gamma irradiation on the properties of PbS thin films. *Radiat. Phys. Chem.* **171**, 108732 (2020)
22. F.G. Hone, F.B. Dejene, *J. Lumin.* **201**, 321–328 (2018)
23. M.T.S. Nair, P.K. Nair, R.A. Zingaro, E.A. Meyers, Enhancement of photosensitivity in chemically deposited CdSe thin films by air annealing. *J. Appl. Phys.* **74**, 1879–1884 (1993)
24. K.C. Preetha, K.V. Murali, A.J. Ragina, K. Deepa, T.L. Remadevi, *Curr. Appl. Phys.* **12**, 5359 (2012)
25. C.S. Barrett, T.B. Massalski, *Crystallographic Methods Principles and Data*, 3rd edn. (McGraw Hill, New York, 1996).
26. M. Shkir, A. Khan, A.M. El-Toni, A. Aldalbahi, I.S. Yahia, S. AlFaify, Structural, morphological, opto-nonlinear-limiting studies on Dy:PbI₂/FTO thin films derived facilely by spin coating technique for optoelectronic technology. *J. Phys. Chem. Solids* **130**, 189–196 (2019)
27. J. Pelleg, E. Elish, Stress changes in chemical vapor deposition tungsten silicide (polycide) film measured by x-ray diffraction. *J. Vac. Sci. Technol. A* **20**, 754–761 (2002)
28. A. Arulanantham, S. Valanarasu, A. Kathalingam, K. Jeyadheepan, *J. Mater. Sci. Mater. Electron.* **29**, 11358–11366 (2018)
29. S. Yilmaz, S.B. Törel, İ. Polat, M.A. Olgar, M. Tomakin, E. Bacaksız, Enhancement in the optical and electrical properties of CdS thin films through Ga and K co-doping. *Mater. Sci. Semicond. Process.* **60**, 45–52 (2017)
30. P. Kubelka, F. Munk, *Z. Tech. Phys.* **12**, 593 (1931)
31. P. Kubelka, New contributions to the optics of intensely light-scattering materials. *J. Opt. Soc. Am.* **38**, 448–457 (1948)
32. J. Tauc, A. Menth, *J. Non-Cryst. Solids* **569**, 8–10 (1972)
33. T. Kako, N. Kikugawa, J. Ye, Photocatalytic activities of AgSbO₃ under visible light irradiation. *Catal. Today* **131**, 197–202 (2008)
34. H. El-Zahed, The effect of γ -doses on the optical band gap of AgInSe₂ films. *J. Phys. Chem. Solids* **62**, 641–646 (2001)
35. H.A. Wahab, A.A. Salama, A.A. El-Saeid, O. Nur, M. Willander, I.K. Battisha, Optical, structural and morphological studies of (ZnO) nano-rod thin films for biosensor applications using sol gel technique. *Results Phys.* **3**, 46–51 (2013)
36. T.K. Maity, S.L. Sharma, Effect of gamma radiation on optical and electrical properties of tellurium dioxide thin films. *Bull. Mater. Sci.* **31**, 841–846 (2008)
37. L. Xue, L. Xaing, L.P. Ting, C.X. Wang, L. Ying, C.C. Bao, Mg doping reduced full width at half maximum of the near-band-edge emission in Mg doped ZnO films. *Chin. Phys. B* **19**, 027202 (2010)
38. M. Sailai, A. Aierken, L. Qiqi, M. Heini, X. Zhao, J. Mo, G. Jie, R. Hao, Z. Yu, G. Qi, *Semiconductors* **54**, 554–557 (2020)
39. A. Echresh, C.O. Chey, M.Z. Shoushtari, V. Khranovskyy, O. Nur, M. Willander, UV photo-detector based on p-NiO thin film/n-ZnO nanorods heterojunction prepared by a simple process. *J. Alloys Compd.* **632**, 165 (2015)
40. S.M. Ali, S.M. Ramay, N.U. Rehman, T.S. AlKhuraiji, M.A. Shar, A. Mahmood, A. Hassan, M. Riaz, Investigation of gamma irradiation effects on the properties of CdS/p-Si heterostructure. *Mater. Sci. Semicond. Process.* **93**, 44–49 (2019)
41. Z. Yuan, A photodiode with high rectification ratio and low turn-on voltage based on ZnO nanoparticles and SubPs planar heterojunction. *Phys. E* **56**, 160–164 (2014)
42. K. Ejderha, N. Yildirim, A. Turat, *Superlattice Microstruct.* **47**, 241 (2010)
43. S.M. Sze, *Physics of Semiconductor Devices* (Wiley Eastern, New York, 1993).
44. A. Kumar, S. Arafin, M.C. Amann, R.S. Singh, Temperature dependence of electrical characteristics of Pt/GaN Schottky diode fabricated by UHV E-beam evaporation. *Nanoscale Res. Lett.* **8**, 481 (2013)
45. S.K. Cheung, N.W. Cheung, Extraction of Schottky diode parameters from forward current-voltage characteristics. *Appl. Phys. Lett.* **49**, 85–87 (1986)
46. K.P. Hsueh, Temperature dependent current-voltage characteristics of n-MgxZn1-xO/p-GaN junction diodes. *Microelectron. Eng.* **88**, 1016–1018 (2011)
47. C.S. Tan, H.S. Chen, C.Y. Chiu, S.C. Wu, L.J. Chen, M.H. Huang, Facet-dependent electrical conductivity properties of PbS nanocrystals. *Chem. Mater.* **28**, 1574–1580 (2016)

Publisher's Note Springer Nature remains neutral with regard to jurisdictional claims in published maps and institutional affiliations.